Geophysical Research Letters

RESEARCH LETTER
10.1029/2018GL078172

Key Points:
- Fossil fuel CO_2 emissions drive changes in future ocean $\Delta^{14}C$
- Air-sea flux and interior gradients in ocean $\Delta^{14}C$ reverse sign in high-emission scenarios
- Simulations can guide ongoing ocean observation programs

Supporting Information:
- Supporting Information S1

Correspondence to:
S. Khatiwala,
samar.khatiwala@earth.ox.ac.uk

Citation:
Khatiwala, S., Graven, H., Payne, S., & Heimbach, P. (2018). Changes to the air-sea flux and distribution of radiocarbon in the ocean over the 21st century. *Geophysical Research Letters*, *45*, 5617–5626. https://doi.org/10.1029/2018GL078172

Received 4 APR 2018
Accepted 22 MAY 2018
Accepted article online 29 MAY 2018
Published online 12 JUN 2018

Changes to the Air-Sea Flux and Distribution of Radiocarbon in the Ocean Over the 21st Century

Samar Khatiwala[1], Heather Graven[2], Sarah Payne[1,3], and Patrick Heimbach[4]

[1]Department of Earth Sciences, University of Oxford, Oxford, UK, [2]Department of Physics, Imperial College London, London, UK, [3]Now at Risk Management Solutions, London, UK, [4]Institute for Computational Engineering and Sciences, University of Texas at Austin, Austin, TX, USA

Abstract We investigate the spatiotemporal evolution of radiocarbon ($\Delta^{14}C$) in the ocean over the 21st century under different scenarios for anthropogenic CO_2 emissions and atmospheric CO_2 and radiocarbon changes using a 3-D ocean carbon cycle model. Strong decreases in atmospheric $\Delta^{14}C$ in the high-emission scenario result in strong outgassing of ^{14}C over 2050–2100, causing $\Delta^{14}C$ spatial gradients in the surface ocean and vertical gradients between the surface and intermediate waters to reverse sign. Surface $\Delta^{14}C$ in the subtropical gyres is lower than $\Delta^{14}C$ in Pacific Deep Water and Southern Ocean surface water in 2100. In the low-emission scenario, ocean $\Delta^{14}C$ remains slightly higher than in 1950 and relatively constant over 2050–2100. Over the next 20 years we find decadal changes in $\Delta^{14}C$ of −30‰ to +5‰ in the upper 2 km of the ocean, which should be detectable with continued hydrographic surveys. Our simulations can help in planning future observations, and they provide a baseline for investigating natural or anthropogenic changes in ocean circulation using ocean $\Delta^{14}C$ observations and models.

Plain Language Summary The carbon content and acidity of the ocean are increasing as the ocean has absorbed roughly a third of the CO_2 emitted by the burning of fossil fuels. Human activities are also changing the isotopic composition of carbon in the atmosphere and ocean. In the midtwentieth century, nuclear weapons testing produced a large amount of ^{14}C (radiocarbon), the heavy radioactive isotope of carbon that is extensively used for archeological dating. At the same time, the combustion of fossil fuels reduces the amount of ^{14}C relative to the more common isotope ^{12}C, since fossil fuels have lost all their radiocarbon through radioactive decay. As time passes since the bomb testing, fossil fuel emissions are becoming an increasingly dominant influence on the carbon isotope composition of the atmosphere and ocean. Here we use a computer model to simulate how this composition is likely to evolve over the coming century in response to continued fossil fuel burning. Our results show that by the end of the century surface ocean waters will be more depleted in radiocarbon than deeper waters, a complete reversal of the pattern that prevailed before humans started changing the environment.

1. Introduction

The carbon content and acidity of the ocean are increasing as the ocean has absorbed roughly a third of the CO_2 emitted by fossil fuel combustion and land use change (Khatiwala et al., 2009, 2013; Le Quéré et al., 2016; Sabine et al., 2004). Human activities are also changing the isotopic composition of carbon in the atmosphere and ocean. In the 1950s and 1960s, nuclear weapons testing produced a large amount of radiocarbon (^{14}C) that increased the ratio of $^{14}C/C$ ($\Delta^{14}C$) in atmospheric CO_2. This was a large perturbation to the natural radiocarbon cycle in which radiocarbon is produced in the upper atmosphere through cosmic ray spallation (e.g., Levin & Hesshaimer, 2000), whereupon it is oxidized to CO_2 and participates in the carbon cycle, in particular, entering the ocean through air-sea gas transfer. As "bomb ^{14}C" similarly mixed into the ocean it increased the $\Delta^{14}C$ of oceanic dissolved inorganic carbon (Broecker et al., 1985; Druffel & Linick, 1978). At the same time, the combustion of fossil fuels reduces $\Delta^{14}C$, since fossil fuels have lost all their ^{14}C through radioactive decay (Suess, 1955). As time passes since the bomb testing, fossil fuel emissions are becoming an increasingly dominant influence on atmospheric and oceanic $\Delta^{14}C$ (Graven, 2015; Graven, Guilderson, & Keeling, 2012; Levin et al., 2010).

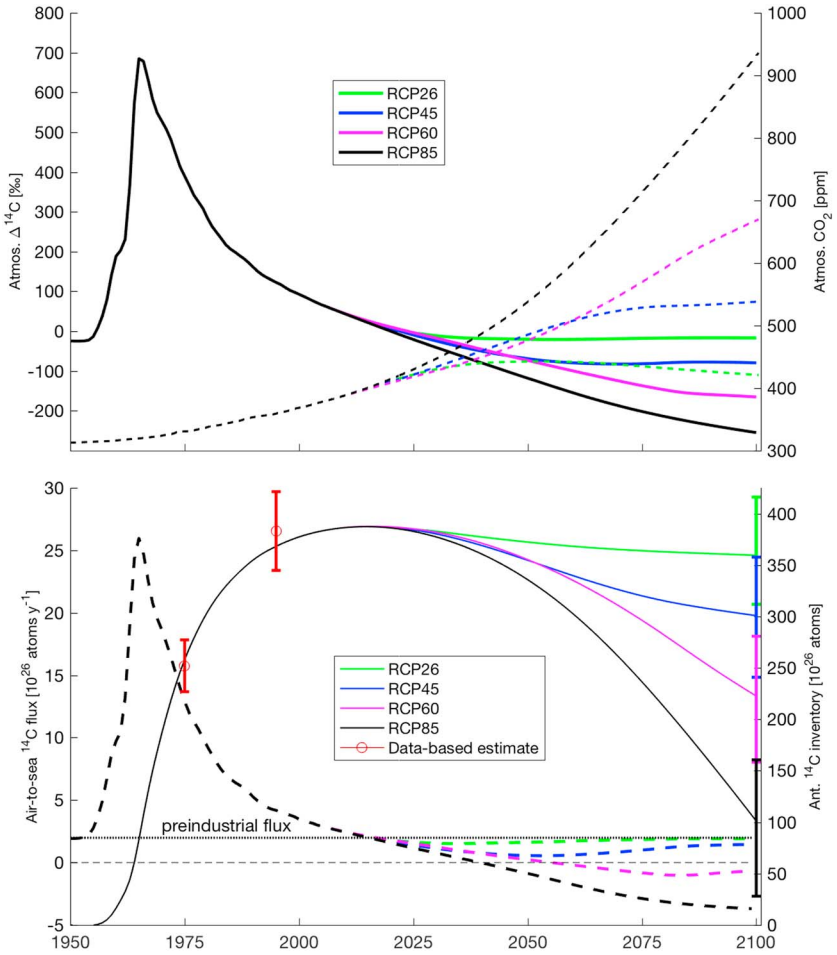

Figure 1. (top panel) Historical and future atmospheric radiocarbon concentration (solid lines and left axis) and CO_2 (dashed lines and right axis) for the four Representative Concentration Pathways from the box diffusion model of Graven (2015) (her midrange estimate) used to drive the ECCO-TM ocean carbon cycle model in the present study. (bottom panel) Corresponding air-to-sea flux (dashed lines and left axis) and oceanic inventory (solid lines and right axis) of ^{14}C simulated by the ECCO-TM model. Vertical lines on the right-hand side show the range in inventory simulated by the box diffusion model, and symbols show data-based estimates of the inventory (Naegler, 2009).

Estimates of the natural ^{14}C distribution present before the Industrial Revolution help to quantify the transport of surface waters into the interior, since the radioactive decay of ^{14}C with a half-life of 5700 years produces measurable depletions in $\Delta^{14}C$ over the centennial time scales of large-scale ocean circulation. Natural $\Delta^{14}C$ has thus been extensively used to construct data-based inverse ocean models (DeVries & Primeau, 2011; Gebbie & Huybers, 2012; Khatiwala et al., 2012; Schlitzer, 2007), reconstruct the history of ocean uptake of anthropogenic CO_2 over the industrial era (Khatiwala et al., 2009), and to evaluate ocean general circulation models (Matsumoto et al., 2004; Toggweiler et al., 1989).

A powerful application of bomb ^{14}C has been its constraint on the global average air-sea gas transfer velocity and CO_2 flux (Sweeney et al., 2007; Wanninkhof, 1992), as well as on gas transfer parameterizations (Naegler, 2009; Wanninkhof, 2014). Observations of recent $\Delta^{14}C$ changes, which are driven by both bomb and fossil fuel influences, have been used to evaluate ocean models' shallow-to-deep transport and anthropogenic CO_2 uptake (Graven, Gruber, et al., 2012, Orr et al., 2001).

Future changes in $\Delta^{14}C$ in response to continued emission of CO_2 have been investigated in previous studies using simple carbon cycle models (Caldeira et al., 1998; Graven, 2015). Increases in fossil fuel emissions are projected to strongly decrease atmospheric and oceanic $\Delta^{14}C$ and cause a net efflux of ^{14}C from the ocean to the atmosphere. Reductions in fossil fuel emissions could alternately lead to approximate stabilization of atmospheric and oceanic $\Delta^{14}C$ (Graven, 2015). These simulations used one-dimensional ocean models and therefore only resolve global changes in the vertical structure of ocean $\Delta^{14}C$.

Here we use an ocean carbon cycle model coupled to a circulation state estimate to examine the changing spatiotemporal distribution of ocean $\Delta^{14}C$ and air-sea ^{14}C fluxes over this century. As atmospheric forcing, we use the atmospheric CO_2 for the four Representative Concentration Pathways (RCPs; van Vuuren et al., 2011) and the corresponding $\Delta^{14}C$ in atmospheric CO_2 simulated by Graven (2015; Figure 1). Our simulations indicate that continued emission of fossil fuel CO_2 over the 21st century will, under the more extreme scenarios, cause a large-scale reversal in the air-sea flux and oceanic distribution of ^{14}C compared with their historical patterns. Even over the next 20 years, decadal changes of 10‰–30‰ are simulated, underscoring the need and opportunity for continued and systematic measurements of ocean ^{14}C dynamics.

2. Methods

To investigate the evolution of ^{14}C in the ocean in response to specified atmospheric concentrations of CO_2 and ^{14}C, we used an abiotic ocean carbon cycle model coupled to the transport matrix method (TMM), a computationally efficient framework for off-line simulation of ocean chemical and biological tracers (Khatiwala, 2007, 2018; Khatiwala et al., 2005). The TMM exploits the fact that the advective-diffusive transport of a passive tracer, including subgrid-scale parameterizations, can be represented as a sequence of sparse matrix-vector products, with "transport matrices" (TMs) extracted from an ocean general circulation model. Here we use a circulation derived from the Estimating the Circulation and Climate of the Ocean (ECCO) state estimate (Stammer et al., 2004), which is based on a 1° horizontal resolution configuration of MITgcm (Marshall et al., 1997) with 21 vertical layers. ECCO uses an adjoint approach to minimize the misfit between the model and a range of hydrographic, current meter, and altimeter data by adjusting heat, momentum, and freshwater fluxes (Wunsch & Heimbach, 2007). TMs representing a monthly mean climatology over the 1992–2004 estimation period were extracted and used for the off-line simulations (ECCO-TM). It should be noted that, while oceanic tracers such as CFCs and radiocarbon were not assimilated, the simulation of ^{14}C in ECCO was extensively investigated by Graven, Gruber, et al. (2012). They found that while the preindustrial surface ocean $\Delta^{14}C$ simulated by ECCO generally matches the observations, surface $\Delta^{14}C$ in the 1970s has a negative bias relative to data, which subsequently decreases through the 1990s. This comparison suggests that shallow-to-deep exchange (via both isopycnal and diapycnal mixing processes) may be too efficient in ECCO.

The carbon cycle model simulates dissolved inorganic carbon (DIC) and ^{14}C in DIC using the Ocean Carbon-Cycle Model Intercomparison Project-Phase 2 protocols for air-sea gas exchange and carbonate chemistry (Orr & Najjar, 1999), as updated for the Ocean Model Intercomparison Project and Coupled Model Intercomparison Project-Phase 6 (CMIP6) by Orr et al. (2017). Briefly, DIC and DI^{14}C enter the ocean from the atmosphere via fluxes that depend on local wind speed, temperature, salinity, sea ice concentration, and carbonate chemistry. In the present simulations, the 6-hourly, climatological wind speed from the CORE-II atmospheric reanalysis (Large & Yeager, 2004) was used to calculate the gas transfer coefficient, with all other variables being taken from the ECCO 1992–2004 climatology. The transfer coefficient is parameterized as a quadratic function of the local wind speed (Wanninkhof, 1992), with a proportionality constant that gives a global mean gas exchange velocity of $\approx$17 cm/hr, in line with recent studies (Naegler, 2009; Wanninkhof, 2014). To investigate the sensitivity of our results to this parameter, additional experiments with mean exchange velocities of 13.5 cm/hr and 20.5 cm/hr, spanning the range of uncertainty (Wanninkhof, 2014), were also carried out (see supporting information S1).

Simulations were performed in three steps. First, for a fixed preindustrial atmospheric CO_2 mixing ratio of 277.89 ppm and $\Delta^{14}C$ of 0‰, a periodic (seasonally repeating) equilibrium state of the carbon cycle model was found using a Newton-Krylov approach (Khatiwala, 2008). Next, the model was integrated from 1765 to 2005 with historical atmospheric CO_2 and $\Delta^{14}C$ data from Meinshausen et al. (2017) and Graven et al. (2017), respectively. Lastly, four separate runs were performed, one for each RCP, for the period 2005 to 2100. For these runs, atmospheric CO_2 was prescribed from the respective RCP (van Vuuren et al., 2011), whereas $\Delta^{14}C$ was taken from the corresponding simulations of Graven (2015). The latter were performed using a coupled one-box atmosphere, one-box land biosphere, and 1-D ocean box diffusion model forced by historical and RCP CO_2, fossil fuel, and land use emissions. For each emission trajectory, the box model was run with a range of values for several parameters, including the ocean eddy diffusivity and gas exchange velocity, resulting in a range of projections for atmospheric (and oceanic) $\Delta^{14}C$. In this study we used the midrange estimate of atmospheric $\Delta^{14}C$ to force the ECCO-TM carbon cycle model and also carried out experiments (see supporting information S1) with the minimum and maximum of the simulated range to assess the uncertainty arising from using a box model-derived atmospheric $\Delta^{14}C$ to drive the ECCO-TM carbon cycle model.

The ECCO-TM simulations do not include any variability in ocean circulation or account for future changes in CO_2 solubility due to increasing temperature. To investigate the impact of such changes, we performed sensitivity experiments (see supporting information S1) with the University of Victoria Earth System Climate Model version 2.9 (UVic ESCM; Eby et al., 2009; Weaver et al., 2001) forced with historical and RCP8.5 atmospheric CO_2 from 1765 to 2100. UVic ESCM is a coarse-resolution (1.8° × 3.6° × 19 ocean depth layers) ocean-atmosphere-biosphere-cryosphere-geosphere model. The preindustrial equilibrium state of the ocean component of this model with regard to hydrographic, radiocarbon, and biogeochemical fields is described in Kvale et al. (2017). As seen in other climate models (e.g., Cheng et al., 2013), greenhouse warming leads to a slowdown in the meridional overturning circulation, in UVic ESCM's case by ~25% between 1765 and 2100 (Figure S8), as well as a reduction in sea ice. To examine the impact of these changes on oceanic $\Delta^{14}C$, two sets of off-line carbon cycle simulations driven by historical and RCP8.5 atmospheric CO_2 and $\Delta^{14}C$ were carried out. The first used fixed, monthly mean TMs and temperature, salinity, and sea ice concentration fields extracted from the preindustrial equilibrium state (Kvale et al., 2017), whereas the second used the corresponding time-varying fields from the transient climate model run.

3. Results

3.1. Air-Sea Flux and Ocean Inventory of ^{14}C

In the preindustrial equilibrium state, the net flux of ^{14}C into the ocean was positive to balance radioactive decay within the ocean. This balance was perturbed by the injection of bomb radiocarbon into the atmosphere, with a dramatic increase in the air-sea flux of ^{14}C and a corresponding increase in the oceanic inventory of anthropogenic ^{14}C (Figure 1), defined as the accumulation of radiocarbon since 1950 (Broecker et al., 1985). Largely due to absorption by the ocean, the anthropogenic ^{14}C spike in the atmosphere has dissipated over the last few decades, leading to a reduced air-sea concentration gradient—and thus flux—over time. Correspondingly, the increase in the global ocean ^{14}C inventory slowed. At the same time, ocean ^{14}C continues to be redistributed from the upper ocean to the deep ocean via ocean circulation (Graven, Gruber, et al., 2012). The simulated inventory for the historical period is in line with data-based estimates (Naegler, 2009).

In response to decreasing atmospheric $\Delta^{14}C$, the net air-sea flux returns to its preindustrial value and the global ocean ^{14}C inventory stops increasing between 2015 (for RCP8.5) and 2017 (for RCP2.6) in our simulations. As seen in Figure 2, the globally integrated flux conceals a strong latitudinal dependence, with low-latitude outgassing of ^{14}C counteracting continued high-latitude uptake. The flux at low latitudes reaches its corresponding preindustrial value earlier compared with middle and high latitudes. The Southern Ocean flux does not return to its prebomb value by 2100 in these simulations.

The precise time at which the flux returns to its preindustrial value depends somewhat on the gas exchange velocity and prescribed atmospheric $\Delta^{14}C$. Sensitivity experiments (Figure S1 in the supporting information) show that this occurs (for RCP8.5) in 2009 and 2022 with exchange velocities of 13.5 cm/hr and 20.5 cm/hr, respectively. And when the model is forced with the minimum and maximum atmospheric $\Delta^{14}C$ of the range of RCP8.5 projections of Graven (2015), the transition occurs in 2012 and 2019, respectively. The results also depend on ocean circulation. As mentioned above, exchange between the upper and deep oceans is perhaps more vigorous in ECCO than supported by observations (Graven, Gruber, et al., 2012). Another 3-D model displaying the opposite bias of too weak shallow-to-deep exchange (Graven, Gruber, et al., 2012) indicates that the global ocean ^{14}C inventory may have already stopped increasing and started to decrease in the mid-2000s. Variability in circulation is another factor to consider. In our simulations with fixed and time-varying circulations with UVic ESCM (Figure S9 in the supporting information), the transition occurs in 2022 and 2017, respectively. The reason for the earlier reversion to preindustrial conditions in the latter, anthropogenically forced case, relative to the fixed circulation run is the slowdown in the meridional overturning circulation from 1850 onward, leading to less uptake of bomb ^{14}C. Given these results, we put the uncertainty in the timing at roughly a decade.

The evolution of the ocean ^{14}C flux and inventory after 2020 are strongly governed by the particular RCP scenario (Graven, 2015). In the RCP2.6 scenario in which atmospheric $\Delta^{14}C$ is projected to remain more or less constant at just below 0‰, the net flux undershoots the preindustrial flux slightly before recovering and leveling off at its preindustrial value. The inventory of anthropogenic ^{14}C in the ocean, however, decreases very slightly from its peak over the rest of the century. This represents a near balance between the continued uptake of ^{14}C in the Southern Ocean and reduced uptake or excess outgassing in the rest of the ocean (Figure 2). In this scenario, while the global inventory of anthropogenic ^{14}C in the ocean remains relatively

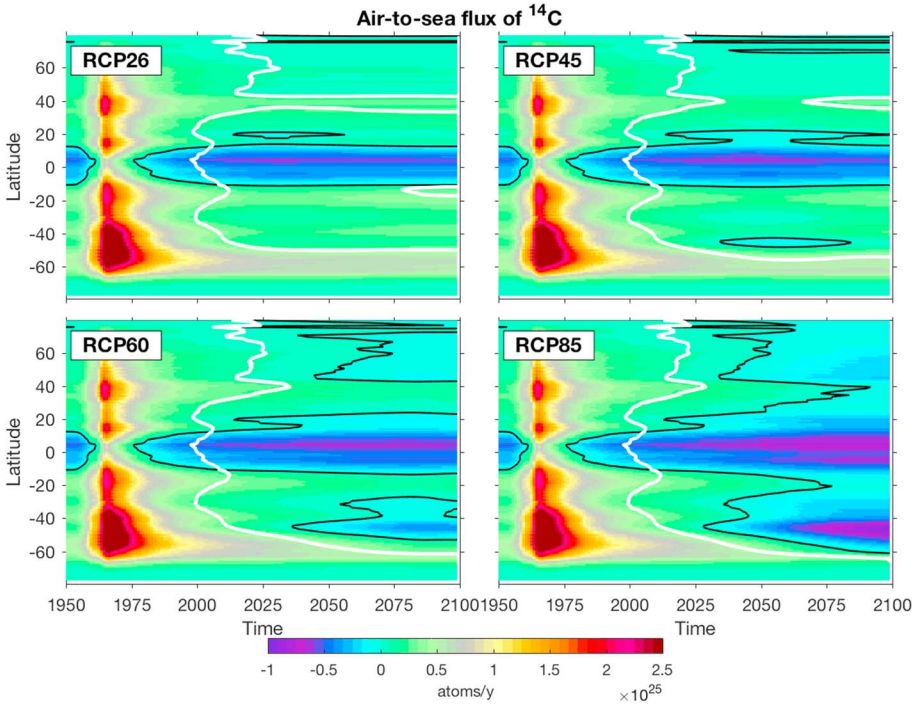

Figure 2. Time-latitude Hovmueller plot of zonally integrated air-to-sea flux of ^{14}C for the four RCP forcing scenarios. The flux is shown as shaded colors, with black contour lines indicating a flux of zero and white contour lines the value of the preindustrial flux.

steady, the anthropogenic ^{14}C continues to be redistributed through the ocean through ocean circulation and through air-sea fluxes.

At the other extreme is RCP8.5, in which sustained CO_2 emissions drive atmospheric Δ^{14}C to below −200‰ by 2100. The global air-sea flux of ^{14}C in RCP8.5 continues to fall to well below its preindustrial value so that the ocean becomes a strong net source of ^{14}C to the atmosphere in ∼2040, as also found by Graven (2015). This persistent outgassing starts in the tropics and expands poleward with time (Figure 2), increasing in magnitude over the duration of the simulation so that, by 2100, the ocean inventory of ^{14}C falls to well under a third of its peak value above the prebomb level.

The other two RCP scenarios fall in between these two extremes. In RCP4.5, with an atmospheric Δ^{14}C projected to be −90‰ in 2100, the air-sea flux reaches a minimum in ∼2055 before increasing toward the preindustrial equilibrium value. On the other hand, in RCP6.0 (Δ^{14}C in 2100 of ∼ −180‰) the air-sea flux reverses sign in 2055. This is consistent with the work of Caldeira et al. (1998) who used a simple one-dimensional box diffusion ocean model forced with the nearly identical "business-as-usual" IPCC IS92a scenario. The flux continues to decrease before reaching a minimum in 2085. In all scenarios the ocean ^{14}C inventory continues to decrease over the course of the simulation, with that in RCP2.6 nearly leveling off by 2100.

While our approach of using atmospheric Δ^{14}C from a box model to drive the ECCO-TM carbon cycle model circumvents the need to perform computationally expensive simulations with a fully coupled 3-D model forced by emissions, which would additionally require a continental biosphere model, it does raise the question of consistency between the box and 3-D ocean circulation models. While it is not straightforward to compare shallow-to-deep transport between the two (e.g., as noted by Caldeira et al., 2002, the box diffusion model treats downward and upward transport symmetrically), for the historical period the range in anthropogenic CO_2 inventory in 1995 simulated by the box model (98–130 PgC; Graven, 2015) is comparable to that in ECCO-TM (121.6 PgC), while the range in ^{14}C inventory in 1995 relative to 1950 simulated by the box model is 339–417 × 10^{26} atoms, compared to 377 × 10^{26} atoms in ECCO-TM. For the future projections, the global ocean ^{14}C inventories predicted by ECCO-TM in 2100 lies almost exactly in the middle of the range simulated by the box model (vertical lines in Figure 1), and our sensitivity runs (Figure S1 in the

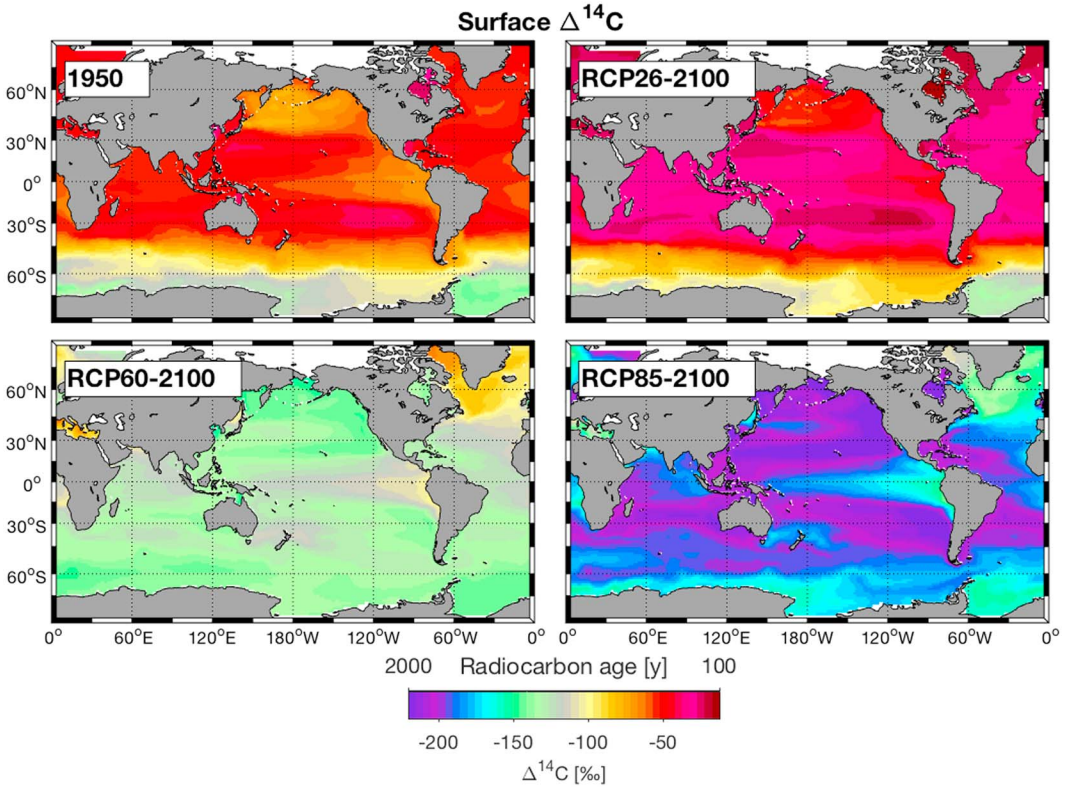

Figure 3. Surface layer $\Delta^{14}C$ in 1950 (top left) and 2100 for the RCP2.6, 6.0, and 8.5 emission scenarios showing progressive depletion of surface waters with fossil fuel emissions. (Figure S2 in the supporting information shows the corresponding plot for RCP4.5.) For perspective, the color scale shows $\Delta^{14}C$ in both permil and conventional radiocarbon age.

supporting information) span the box model's range. Taken together, these results suggest that if one replaced the 1-D ocean model in Graven (2015) by ECCO-TM, the predicted atmospheric radiocarbon pathway for a given RCP CO_2 concentration scenario would lie within the range from Graven (2015).

3.2. Distribution of $\Delta^{14}C$ in 2100

Compared with the $\Delta^{14}C$ distribution in 1950, the predicted $\Delta^{14}C$ in surface water and decadally ventilated water masses is either somewhat higher (RCP2.6) or substantially lower (RCP4.5, RCP6.0 and RCP8.5) in 2100 (Figures 3, 4, S2, and S3). For RCP2.6, $\Delta^{14}C$ is about 20‰–30‰ higher that than in 1950 in the surface ocean, throughout most of the Atlantic and Southern Oceans, and down to about 2,000 m in the Pacific Ocean. In this scenario, it appears that perturbations to ocean $\Delta^{14}C$ from bomb testing and fossil fuel emissions have more or less equilibrated in decadally ventilated regions of the ocean after the period 2050–2100, when atmospheric $\Delta^{14}C$ remains nearly constant.

Large changes in ocean $\Delta^{14}C$ are simulated in the RCP8.5 scenario. In 2100, in RCP8.5, the lowest $\Delta^{14}C$ in the surface ocean is found in the subtropical gyres and midlatitudes, a complete reversal of the pattern in 1950 (Figure 3). In the preindustrial period through the bomb period, surface waters in upwelling regions such as the equator and Southern Ocean have been characterized by low $\Delta^{14}C$ and large conventional radiocarbon ages, due to mixing with deeper ^{14}C-depleted water (Broecker & Peng, 1982; Toggweiler et al., 1989). In contrast, these regions, along with the North Atlantic, show the highest $\Delta^{14}C$ in 2100 in RCP8.5. Even more remarkably, surface waters are now as low in $\Delta^{14}C$ as the deep North Pacific (−200‰), and the highest $\Delta^{14}C$ (−130‰ to −70‰) is found at intermediate depths of ≈500–1,000 m in the Pacific Ocean and at 1,000–3,000 m in the Atlantic Ocean (Figure 4). This strong *U-shaped* pattern of $\Delta^{14}C$ with depth, also seen in simulations with a 1-D box diffusion model (Graven, 2015), is present in all ocean basins but is most prominent in the North Atlantic Ocean. North Atlantic Deep Water shows a "blob" of water relatively enriched in ^{14}C (i.e., younger) near 30°N, where the difference between the surface and 2,000 m is as large as −160‰. Relatively

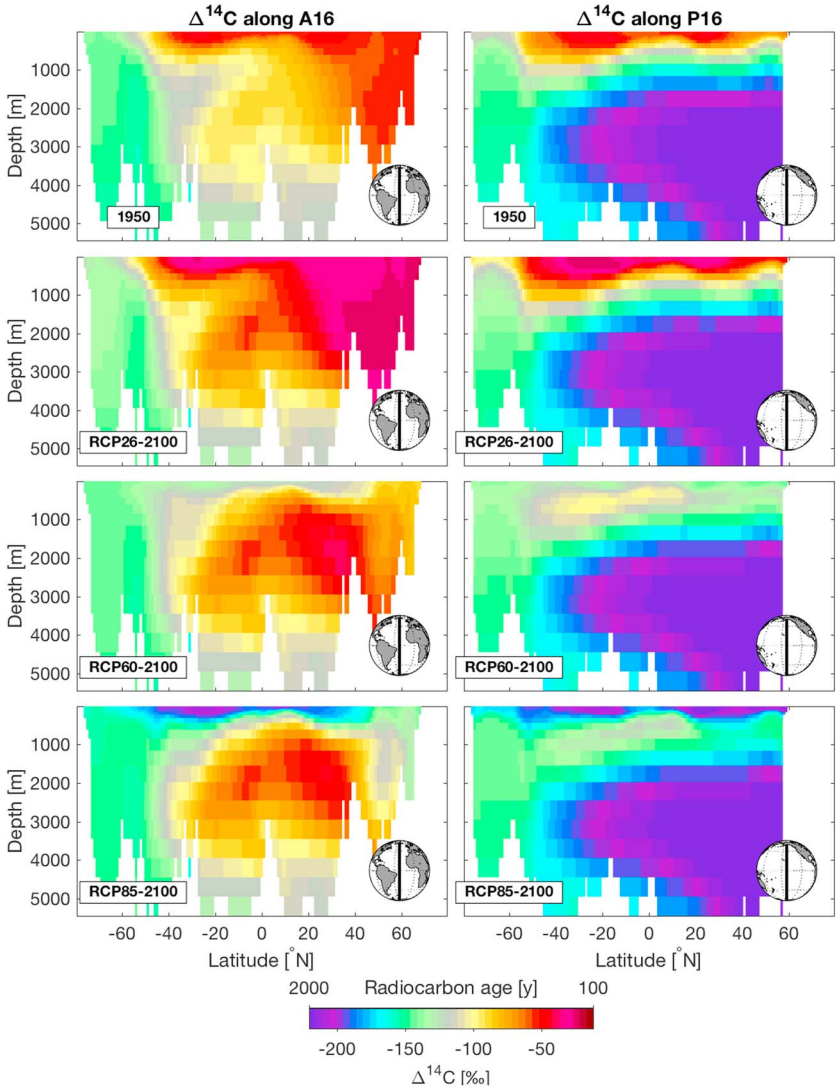

Figure 4. Interior $\Delta^{14}C$ simulated by the carbon cycle model along 30°W in the Atlantic (left panels) and 150°W in the Pacific (right panels), coinciding with repeat hydrography sections A16 and P16, respectively. Data are shown for 1950 (top) and 2100 for the RCP2.6, 6.0, and 8.5 emission scenarios. (Figure S3 of the supporting information shows the corresponding plot for RCP4.5.)

high $\Delta^{14}C$ in North Atlantic surface waters suggests that some ^{14}C reemerges via the North Atlantic ventilation pathway that is often associated only with downwelling, a conclusion supported by the extremely high outgassing flux in that region (Figure S4 in the supporting information).

Simulated changes in ocean $\Delta^{14}C$ in the intermediate scenarios RCP4.5 and RCP6.0 lie between the two extreme scenarios. In RCP6.0 there is very little spatial variation in surface ocean $\Delta^{14}C$ in 2100, with $\Delta^{14}C$ between −150‰ and −100‰ except in the North Atlantic Ocean where $\Delta^{14}C$ is higher. No clear gradient is found in the Southern Ocean, in contrast to the other scenarios and to the historical period. The vertical gradient in $\Delta^{14}C$ in RCP6.0 is reversed in the Atlantic Ocean but not in the Pacific Ocean or the Southern Ocean.

As shown in Figures S5 and S6 in the supporting information, the above results are relatively insensitive to both the gas exchange velocity and prescribed atmospheric $\Delta^{14}C$ (within the range projected by Graven, 2015), with the largest differences seen in the tropics. However, relative to the magnitude of the projected changes, these differences are quite small. Indeed, even large potential future changes in ocean circulation have only a minor impact on the simulated $\Delta^{14}C$ field in 2100 (Figures S10 and S11), suggesting that our results are quite robust.

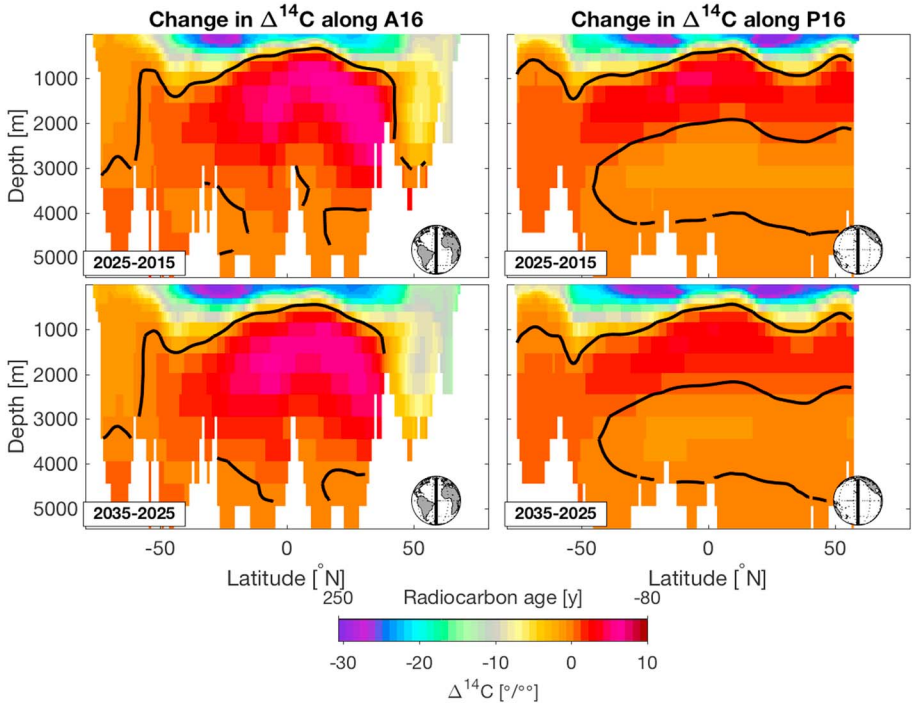

Figure 5. Decadal changes in $\Delta^{14}C$ between 2015–2025 (top) and 2025–2035 (bottom) in the RCP8.5 scenario along 30°W in the Atlantic (left) and 150°W in the Pacific (right). The solid black line is the zero contour where $\Delta^{14}C$ does not change.

3.3. Near-Term Decadal Changes in $\Delta^{14}C$ Distribution

What do these simulations predict for near-term changes in $\Delta^{14}C$ that may be measured by the decadal repeat hydrographic program (GO-SHIP; Talley et al., 2016)? The pattern of change in the RCP8.5 simulations over 2015–2025 and 2025–2035 (Figure 5) is very similar to that found by Graven, Gruber, et al. (2012) for the past two decades from observations and model simulations. $\Delta^{14}C$ decreases in shallow layers (which Graven, Gruber, et al., 2012, define as potential density anomaly, $\sigma_\theta < 26.5$) due to ^{14}C transport into the deep ocean as well as ^{14}C outgassing to the atmosphere, whereas $\Delta^{14}C$ increases in deeper layers. Simulated changes using other scenarios are very similar to RCP8.5 until 2030 and not shown here. Surface ocean $\Delta^{14}C$ decreases by as much as 30‰ between 2015 and 2025 and by slightly more over the following decade. In contrast, $\Delta^{14}C$ of water between 1000–3000 m in the North Atlantic and 1000–2000 m in the North Pacific show decadal increases of about 10‰. The $\Delta^{14}C$ changes predicted over broad regions of the ocean are much larger than a typical measurement uncertainty of 2‰–3‰ and thus easily detectable. Over much of the ocean, these changes are also larger than the uncertainty due to gas exchange velocity and projected atmospheric radiocarbon concentration (Figure S7 in the supporting information). The recent changes in $\Delta^{14}C$ simulated by ECCO-TM were found to be weaker in magnitude than the observed changes, and weaker in magnitude than the changes simulated by another ocean model, which was attributed to a relatively rapid rate of shallow-to-deep exchange in ECCO-TM (Graven, Gruber, et al., 2012). Therefore, we expect that the near-term $\Delta^{14}C$ changes are sensitive to model transport and those simulated here may be somewhat weaker in magnitude than those that will be observed or simulated by another ocean model.

4. Summary and Conclusions

This study uses an ocean carbon cycle model to investigate, for the first time, the spatiotemporal evolution of radiocarbon in the ocean in response to future anthropogenic CO_2 emissions and changes in atmospheric CO_2 and $\Delta^{14}C$. In most emission scenarios, the oceanic inventory of ^{14}C decreases over the course of the simulation, the exception being RCP2.6, which shows a leveling off. In RCP2.6, the global air-sea flux of ^{14}C has approximately stabilized near its preindustrial value by 2100, whereas in the more extreme RCP6.0 and RCP8.5 scenarios, the air-sea flux reverses sign, with the ocean becoming a net source of ^{14}C to the atmosphere around midcentury. The trends in inventory and flux are mirrored in the spatial distribution of $\Delta^{14}C$.

In all scenarios except RCP2.6, surface waters become progressively more depleted in ^{14}C to the extent that by 2100, in the most extreme case of RCP8.5, surface waters in the subtropics and midlatitudes have $\Delta^{14}C$ of less than −200‰, an apparent radiocarbon age of 2000 years. On the other hand, upwelling regions such as the equator and Southern Ocean, which were characterized in the prebomb period by low ^{14}C due to mixing with deeper ^{14}C-depleted water, are projected to have the highest $\Delta^{14}C$ in 2100. This reversal of the historical spatial pattern is also seen in the interior where, by 2100, the depth dependence of $\Delta^{14}C$ resembles a U shape, with highest $\Delta^{14}C$ values (lowest radiocarbon ages) found at intermediate depths. Sensitivity experiments with the UVic ESCM model show that these results are robust to potential future changes in ocean circulation, CO_2 solubility and sea ice induced by anthropogenic warming.

In the near term, the trend of the last few decades toward decreasing $\Delta^{14}C$ values in the upper ocean and increasing $\Delta^{14}C$ in deeper waters documented by Graven, Gruber, et al. (2012) is projected to continue. Specifically, the $\Delta^{14}C$ of surface waters decreases by ∼30‰ between 2015 and 2025 and as much again between 2025 and 2035, whereas waters between 1,000 and 3,000 m show decadal increases of ∼10‰. While our results are based on a single ocean model, the simulated pattern of recent $\Delta^{14}C$ changes in ECCO-TM are similar to observations and to changes simulated by a different ocean model, whereas the magnitude of change varies among models (Graven, Gruber, et al., 2012). Since the ECCO-TM model underestimated the magnitude of observed $\Delta^{14}C$ changes over the previous decade, it may also underestimate the magnitude of observed $\Delta^{14}C$ changes that will occur over the next few decades. Simulations with more ocean models would help to diagnose the sensitivity of simulated future changes in ocean radiocarbon to the model circulation.

It is important to emphasize that the projected changes in $\Delta^{14}C$ described in this study are almost entirely due to the prescribed, time-varying atmospheric CO_2 and radiocarbon concentrations. In particular, the simulations with the ECCO state estimate do not include any variability in ocean circulation and as such provide a useful point of reference against which measurements and other simulations can be compared to potentially identify changes in ocean circulation due to natural variability or anthropogenic climate change (Graven, Gruber, et al., 2012; Rodgers et al., 2011). As suggested by our experiments with the UVic ESCM model, the magnitude of changes in $\Delta^{14}C$ that can be expected from decadal variability in circulation may in the near term be comparable in some places to those arising from atmospheric $\Delta^{14}C$ changes (Druffel & Griffin, 1993; Graven, Gruber, et al., 2012). The work presented here thus highlights the importance of continued observations of radiocarbon in the ocean, particularly over the upper 2,500 m where the largest $\Delta^{14}C$ changes are predicted to occur.

Acknowledgments
We would like to thank Karin Kvale for guidance with the UVic ESCM simulations; two anonymous reviewers for their constructive comments; and the RCP Task Group for providing CO_2 concentration and emission scenarios. S. Khatiwala was supported in part by US NSF grant OCE 12-34971 and UK NERC grant NE/K015613/1. H. Graven acknowledges support from the European Commission through a Marie Curie Career Integration grant. Computing resources were provided by the Climate Simulation Laboratory at NCAR's Computational and Information Systems Laboratory (ark:/85065/d7wd3xhc), sponsored by the National Science Foundation and other agencies, and the University of Oxford Advanced Research Computing (ARC) facility (https://doi.org/10.5281/zenodo.22558). All code and data used to perform the simulations presented here are freely available from the TMM repository (https://github.com/samarkhatiwala/tmm). Model output can be downloaded from http://kelvin.earth.ox.ac.uk/spk/Research/TMM/RadiocarbonGRL2018/.

References

Broecker, W. S., & Peng, T.-H. (1982). Tracers in the sea, Lamont- Doherty Earth Observatory.

Broecker, W. S., Peng, T. H., Ostlund, G., & Stuiver, M. (1985). The distribution of bomb radiocarbon in the ocean. *Journal of Geophysical Research*, *90*, 6953–6970.

Caldeira, K., Rau, G. H., & Duffy, P. B. (1998). Predicted net efflux of radiocarbon from the ocean and increase in atmospheric radiocarbon content. *Geophysical Research Letters*, *25*, 3811–3814.

Caldeira, K., Wickett, M. E., & Duffy, P. B. (2002). Depth, radiocarbon, and the effectiveness of direct CO_2 injection as an ocean carbon sequestration strategy. *Geophysical Research Letters*, *29*, 1766. https://doi.org/10.1029/2001GL014234

Cheng, W., Chiang, J. C. H., & Zhang, D. (2013). Atlantic Meridional Overturning Circulation (AMOC) in CMIP5 models: RCP and historical simulations. *Journal of Climate*, *26*(18), 7187–7197. https://doi.org/10.1175/JCLI-D-12-00496.1

DeVries, T., & Primeau, F. (2011). Dynamically and observationally constrained estimates of water-mass distributions and ages in the global ocean. *Journal of Physical Oceanography*, *41*, 2381–2401. https://doi.org/10.1175/JPO-D-10-05011.1

Druffel, E. M., & Griffin, S. (1993). Large variations of surface ocean radiocarbon: Evidence of circulation changes in the Southwestern Pacific. *Journal of Geophysical Research*, *98*(C11), 20,249–20,259. https://doi.org/10.1029/93JC02113

Druffel, E. M., & Linick, T. W. (1978). Radiocarbon in annual coral rings of Florida. *Geophysical Research Letters*, *5*, 913–916.

Eby, M., Zickfeld, K., Montenegro, A., Archer, D., Meissner, K. J., & Weaver, A. J. (2009). Lifetime of anthropogenic climate change: Millennial time scales of potential CO_2 and surface temperature perturbations. *Journal of Climate*, *22*(10), 2501–2511. https://doi.org/10.1175/2008JCLI2554.1

Gebbie, G., & Huybers, P. (2012). The mean age of ocean waters inferred from radiocarbon observations: sensitivity to surface sources and accounting for mixing histories. *Journal of the Atmospheric Sciences*, *42*, 291–305.

Graven, H. D. (2015). Impact of fossil fuel emissions on atmospheric radiocarbon and various applications of radiocarbon over this century. *Proceedings of the National Academy of Sciences of the United States of America*, *112*, 9542–9545. https://doi.org/10.1073/pnas.1504467112

Graven, H. D., Allison, C., Etheridge, D., Hammer, S., Keeling, R. F., Levin, I., et al. (2017). Historical carbon isotopes in atmospheric CO_2. Version 1.0. Earth system grid federation. https://doi.org/10.22033/ESGF/input4MIPs.1162

Graven, H. D., Gruber, N., Key, R., Khatiwala, S., & Giraud, X. (2012). Changing controls on oceanic radiocarbon: New insights on shallow-to-deep ocean exchange and anthropogenic CO_2 uptake. *Journal of Geophysical Research*, *117*, C10005. https://doi.org/10.1029/2012JC008074

Graven, H. D., Guilderson, T. P., & Keeling, R. F. (2012). Observations of radiocarbon in CO_2 at La Jolla, California, USA 1992–2007: Analysis of the long-term trend. *Journal of Geophysical Research*, *117*, D02302. https://doi.org/10.1029/2011JD016533

Khatiwala, S. (2007). A computational framework for simulation of biogeochemical tracers in the ocean. *Global Biogeochemical Cycles*, *21*, GB3001. https://doi.org/10.1029/2007GB002923

Khatiwala, S. (2008). Fast spin up of ocean biogeochemical models using matrix-free Newton-Krylov. *Ocean Modelling*, *23*, 121–129. https://doi.org/10.1016/j.ocemod.2008.05.002

Khatiwala, S. (2018). Transport Matrix Method software for ocean biogeochemical simulations. https://doi.org/10.5281/zenodo.1246300

Khatiwala, S., Primeau, F., & Hall, T. (2009). Reconstruction of the history of anthropogenic CO_2 concentrations in the ocean. *Nature*, *462*, 346–349. https://doi.org/10.1038/nature08526

Khatiwala, S., Primeau, F., & Holzer, M. (2012). Ventilation of the deep ocean constrained with tracer observations and implications for radiocarbon estimates of ideal mean age. *Earth and Planetary Science Letters*, *325*, 116–125. https://doi.org/10.1016/j.epsl.2012.01.038

Khatiwala, S., Tanhua, T., Mikaloff Fletcher, S., Gerber, M., Doney, S. C., Graven, H. D., et al. (2013). Global ocean storage of anthropogenic carbon. *Biogeosciences*, *10*, 2169–2191. https://doi.org/10.5194/bg-10-2169-2013

Khatiwala, S., Visbeck, M., & Cane, M. (2005). Accelerated simulation of passive tracers in ocean circulation models. *Ocean Modelling*, *9*, 51–69.

Kvale, K. F., Khatiwala, S., Dietze, H., Kriest, I., & Oschlies, A. (2017). Evaluation of the Transport Matrix Method for simulation of ocean biogeochemical tracers. *Geoscientific Model Development*, *10*, 2425–2445. https://doi.org/10.5194/gmd-10-2425-2017

Large, W., & Yeager, S. (2004). Diurnal to decadal global forcing for ocean and sea-ice models: The datasets and flux climatologies (Tech. Rep. NCAR Technical Note: NCAR/TN-460+STR). Boulder, CO: CGD Division of the National Centre for Atmospheric Research.

Le Quéré, C., Andrew, R. M., Canadell, J. G., Sitch, S., Korsbakken, J. I., Peters, G. P., et al. (2016). Global carbon budget 2016. *Earth System Science Data*, *8*(2), 605–649. https://doi.org/10.5194/essd-8-605-2016

Levin, I., & Hesshaimer, V. (2000). Radiocarbon—A unique tracer of global carbon cycle dynamics. *Radiocarbon*, *42*, 69–80.

Levin, I., Naegler, T., Kromer, B., Diehl, M., Francey, R. J., Gomez-Pelaez, A. J., et al. (2010). Observations and modelling of the global distribution and long-term trend of atmospheric $^{14}CO_2$. *Tellus B*, *62*, 26–46.

Marshall, J., Adcroft, A., Hill, C., Perelman, L., & Heisey, C. (1997). A finite-volume, incompressible Navier-Stokes model for studies of the ocean on parallel computers. *Journal of Geophysical Research*, *102*, 5733–5752.

Matsumoto, K., Sarmiento, J. L., Key, R. M., Aumont, O., Bullister, J. L., Caldeira, K., et al. (2004). Evaluation of ocean carbon cycle models with data-based metrics. *Geophysical Research Letters*, *31*, L07303. https://doi.org/10.1029/2003GL018970

Meinshausen, M., Vogel, E., Nauels, A., Lorbacher, K., Meinshausen, N., Etheridge, D., et al. (2017). Historical greenhouse gas concentrations for climate modelling (CMIP6). *Geoscientific Model Development*, *10*, 2057–2116. https://doi.org/10.5194/gmd-10-2057-2017

Naegler, T. (2009). Reconciliation of excess ^{14}C-constrained global CO_2 piston velocity estimates. *Tellus B*, *61*, 372–384.

Orr, J. C., Maier-Reimer, E., Mikolajewicz, U., Monfray, P., Sarmiento, J. L., Toggweiler, J. R., et al. (2001). Estimates of anthropogenic carbon uptake from four three-dimensional global ocean models. *Global Biogeochemical Cycles*, *15*, 43–60.

Orr, J. C., & Najjar, R. G. (1999). Abiotic-HOWTO. Internal OCMIP report (Tech. Rep.) Gif-sur-Yvette, France: LSCE/CEA Saclay.

Orr, J. C., Najjar, R. G., Aumont, O., Bopp, L., Bullister, J. L., Danabasoglu, G., et al. (2017). Biogeochemical protocols and diagnostics for the CMIP6 Ocean Model Intercomparison Project (OMIP). *Geoscientific Model Development*, *10*, 2169–2199. https://doi.org/10.5194/gmd-10-2169-2017

Rodgers, K. B., Mikaloff-Fletcher, S. E., Bianchi, D., Beaulieu, C., Galbraith, E. D., Gnanadesikan, A., et al. (2011). Interhemispheric gradient of atmospheric radiocarbon reveals natural variability of Southern Ocean winds. *Climate of the Past*, *7*, 1123–1138. https://doi.org/10.5194/cp-7-1123-2011

Sabine, C. L., Feely, R. A., Gruber, N., Key, R. M., Lee, K., Bullister, J. L., et al. (2004). The ocean sink for anthropogenic CO_2. *Science*, *305*, 367–371.

Schlitzer, R. (2007). Assimilation of radiocarbon and chlorofluorocarbon data to constrain deep and bottom water transports in the world ocean. *Journal of Physical Oceanography*, *37*(2), 259–276.

Stammer, D., Ueyoshi, K., Köhl, A., Large, W. G., Josey, S. A., & Wunsch, C. (2004). Estimating air-sea fluxes of heat, freshwater, and momentum through global ocean data assimilation. *Journal of Geophysical Research*, *109*, C05023. https://doi.org/10.1029/2003JC002082

Suess, H. E. (1955). Radiocarbon concentration in modern wood. *Science*, *122*, 415–417.

Sweeney, C., Gloor, E., Jacobson, A. R., Key, R. M., McKinley, G., Sarmiento, J. L., & Wanninkhof, R. (2007). Constraining global air-sea gas exchange for CO_2 with recent bomb ^{14}C measurements. *Global Biogeochemical Cycles*, *21*, GB2015. https://doi.org/10.1029/2006GB002784

Talley, L. D., Feely, R. A., Sloyan, B. M., Wanninkhof, R., Baringer, M. O., Bullister, J. L., et al. (2016). Changes in ocean heat, carbon content, and ventilation: Review of the first decade of global repeat hydrography (GO-SHIP). *Annual Review of Marine Science*, *8*, 185–215. https://doi.org/10.1146/annurev-marine-052915-100829

Toggweiler, J. R., Dixon, K., & Bryan, K. (1989). Simulations of radiocarbon in a coarse resolution world ocean model, 1. Steady state prebomb distributions. *Journal of Geophysical Research*, *94*, 8217–8242.

van Vuuren, D. P., Edmonds, J., Kainuma, M., Riahi, K., Thomson, A., Hibbard, K., et al. (2011). The representative concentration pathways: An overview. *Climatic Change*, *109*, 5–31. https://doi.org/10.1007/s10584-011-0148-z

Wanninkhof, R. (1992). Relationship between wind speed and gas exchange over the ocean. *Journal of Geophysical Research*, *97*, 7373–7382.

Wanninkhof, R. (2014). Relationship between wind speed and gas exchange over the ocean revisited. *Limnology and Oceanography: Methods*, *12*, 351–362. https://doi.org/10.4319/lom.2014.12.351

Weaver, A., Eby, M., Wiebe, E., Bitz, C., Duffy, P., Ewen, T., et al. (2001). The UVic Earth System Climate model: Model description, climatology, and applications to past, present and future climates. *Atmosphere-Ocean*, *39*, 361–428.

Wunsch, C., & Heimbach, P. (2007). Practical global oceanic state estimation. *Physica D*, *230*, 197–208.